machines

MDPI

Article

Sustainable Cooling Strategies in End Milling of AISI H11 Steel Based on ANFIS Model

Arumugam Balasuadhakar [1], Sundaresan Thirumalai Kumaran [2,*] and Saood Ali [3,*]

[1] Department of Nautical Science, AMET University, Kanathur, Chennai 603112, Tamil Nadu, India; balasudhakar@ametuniv.ac.in
[2] Department of Mechanical Engineering, PSG Institute of Technology and Applied Research, Coimbatore 641062, Tamil Nadu, India
[3] School of Mechanical Engineering, Yeungnam University, 280 Daehak-ro, Gyeongsan 38541, Gyeongbuk, Republic of Korea
* Correspondence: thirumalaikumaran@yahoo.com (S.T.K.); saoodali@ynu.ac.kr (S.A.)

Abstract: In hard milling, there has been a significant surge in demand for sustainable machining techniques. Research indicates that the Minimum Quantity Lubrication (MQL) method is a promising approach to achieving sustainability in milling processes due to its eco-friendly characteristics, as well as its cost-effectiveness and improved cooling efficiency compared to conventional flood cooling. This study investigates the end milling of AISI H11 die steel, utilizing a cooling system that involves a mixture of graphene nanoparticles (Gnps) and sesame oil for MQL. The experimental framework is based on a Taguchi L36 orthogonal array, with key parameters including feed rate, cutting speed, cooling condition, and air pressure. The resulting outcomes for cutting zone temperature and surface roughness were analyzed using the Taguchi Signal-to-Noise ratio and Analysis of Variance (ANOVA). Additionally, an Adaptive Neuro-Fuzzy Inference System (ANFIS) prediction model was developed to assess the impact of process parameters on cutting temperature and surface quality. The optimal cutting parameters were found to be a cutting speed of 40 m/min, a feed rate of 0.01 mm/rev, a jet pressure of 4 bar, and a nano-based MQL cooling environment. The adoption of these optimal parameters resulted in a substantial 62.5% reduction in cutting temperature and a 68.6% decrease in surface roughness. Furthermore, the ANFIS models demonstrated high accuracy, with 97.4% accuracy in predicting cutting temperature and 92.6% accuracy in predicting surface roughness, highlighting their effectiveness in providing precise forecasts for the machining process.

Keywords: sustainable machining; minimum quantity lubrication; ANFIS; graphene nanoparticles

check for updates

Academic Editor: Sheng Li

Received: 18 February 2025
Revised: 12 March 2025
Accepted: 13 March 2025
Published: 14 March 2025

Citation: Balasuadhakar, A.; Kumaran, S.T.; Ali, S. Sustainable Cooling Strategies in End Milling of AISI H11 Steel Based on ANFIS Model. *Machines* **2025**, *13*, 237. https://doi.org/10.3390/machines13030237

Copyright: © 2025 by the authors. Licensee MDPI, Basel, Switzerland. This article is an open access article distributed under the terms and conditions of the Creative Commons Attribution (CC BY) license (https://creativecommons.org/licenses/by/4.0/).

1. Introduction

AISI H11 steel is widely used in the construction of high-performance hot-work tools because of its exceptional wear resilience and heat resistance. Moreover, its preference for aerospace and automotive components is rooted in its capacity to deliver durability and dependability, particularly in settings characterized by elevated temperatures and high stress levels [1]. Compared to similar materials, such as AISI H13 and D2 tool steels, AISI H11 offers a balanced combination of toughness and thermal stability, making it a preferred choice for demanding machining applications [2]. In the hard milling process, the coolant assumes a key role in prolonging the durability of the cutter and elevating the precision of the milled surface. This is accomplished through the reduction in cutting temperatures

and the provision of lubrication within the cutting region [3]. The Minimum Quantity Lubrication (MQL) technique is recognized for its standing among the most sustainable machining methods, effectively mitigating the adverse impact on the environment and reducing costs associated with traditional flood cooling techniques [4].

Vegetable oil cutting fluids, derived from renewable sources, offer eco-friendly machining with excellent lubrication. These fluids ensure a safer work environment owing to low toxicity and high biodegradability. The integration of the MQL system with vegetable oil significantly contributes the sustainable machining practices [5]. In the present era, there is a growing adoption of nano cutting fluids in the MQL method to boost machining performance. The integration of nanoparticles notably enhances the tribological behavior of the cutting fluids [6]. Ross et al. conducted the study to investigate the efficacy of MWCNT suspended soybean oil MQL to compare with other cooling environments such as dry milling, pure MQL, and cryogenic carbon dioxide while machining Monel 400. The results showed that nano-MQL was more efficient than the other cooling environments, leading to lower cutting temperatures, better surface roughness, and reduced flank wear [7]. Another study, conducted by Duc et al., involving soybean oil-derived MQL applied in hard milling of 60Si2Mn steel, utilized a nanofluid prepared with Al_2O_3 nanoparticles. The research identified a significant enhancement in lubrication and cooling performance due to the incorporation of these nanoparticles [8].

Sesame oil, which is widely cultivated and valued for its numerous benefits, possesses excellent lubrication and biodegradability due to its inherent chemical composition [9]. The elevated levels of oleic and linoleic acids, which are unsaturated fatty acids [10], contributes to its effective lubricating properties by forming a stable film that reduces friction between surfaces. Additionally, the presence of natural antioxidants like sesamol and sesamin helps to maintain its stability under operating conditions, preventing the oil from degrading quickly [11]. Compared to other vegetable oils, sesame oil offers additional health benefits for machine operators. Its non-toxic nature and high antioxidant content further reduce the risk of skin irritation and respiratory issues, which can be a concern with some other vegetable oils that may contain higher levels of allergens or irritants [12]. This makes it a safer and more effective choice in machining environments.

Padmini et al. conducted a comparative study on machining AISI 1040 under a MQL environment using sesame oil and coconut oil as base fluids. They incorporated both nano- and microparticles of MoS_2 into the base oils. The study compared the machining performance of both base oil environments with dry machining. The results indicated that sesame oil mixed with nano MoS_2 outperformed coconut oil, achieving an 86% drop in cutting force, a 34% decrease in cutter wear, and a 23% drop in surface roughness relative to dry turning [13]. Furthermore, Ni et al. investigated the use of Fe_3O_4, Al_2O_3, and carbon nanoparticles in a sesame oil-based nanofluid for broaching of AISI 1045 workpiece. Their findings demonstrated that the carbon nanofluid exhibited superior properties, including enhanced viscosity, reduced frictional coefficient, lower broaching load, minimized vibration, and improved surface quality [14].

Graphene nanoplatelets (Gnps) stand out among various nanoparticles, capturing substantial attention from researchers for their remarkable thermal conductivity and superior lubrication characteristics [15]. Haq et al. carried out a study on the milling process of Inconel 718, employing MQL and graphene-based nanofluid MQL (NMQL). Utilizing Response Surface Methodology (RSM), they developed empirical models for material removal rate, surface quality, cutting temperature, and machining power, which were validated through experimental results. The findings indicated that NMQL resulted in a 20.1% reduction in surface roughness, a 14.7% diminution in cutting temperature, and a 13.3% decrease in machining power compared to MQL [16]. Another investigation conducted by Gong

et al. by employing Gnps sized with 15 µm and 5 µm on similar materials. The findings revealed that the smaller size exhibited outstanding results regarding surface smoothness and cutting speed [17]. Moreover, as highlighted in the study conducted by Bertolini et al., the utilization of Gnps with Accu-Lube LB 2000 while machining Inconel 718 leads to reduced flank wear when compared to conventional MQL techniques [18]. Furthermore, another investigation on tool wear was conducted by Wang et al. on the machining of Ti6Al4V alloy using a diamond tool under two different environments: pure water-based MQL with Gnps and dry machining. Their findings indicated that the interface properties between the cutter and workpiece were enhanced by the Gnps in the nano-MQL, effectively preventing direct interaction between the workpiece and the cutter. This modification resulted in a notable decrease in tool wear [19].

Marcon et al. performed an experimental investigation on the micro-milling operation of AISI H13, investigating the impact on cutting force and surface finish quality. The results revealed that the incorporation of Gnps led to notable enhancements in both surface finish and milling force [20]. Moreover, Baldin et al. studied the influence of three distinct base fluids mixed with Gnps in the end milling process of AISI 1045 steel. Analyzing the results through ANOVA and Tukey's test, the study concluded that the incorporation of 0.1 wt.% Gnps enhances lubricating properties, effectively reducing wear mechanisms in vegetable-based oil [21]. In optimizing turning parameters during the machining of M42 steel under both pure MQL and Gnps-mixed MQL systems, Anandan et al. utilized Multi-Objective Optimization by Ratio Analysis combined with the Analytic Hierarchy Process [22].

The shift toward sustainable manufacturing is accelerated by a prominent integration of machine learning and artificial intelligence technologies. This trend signifies a strategic incorporation of advanced computational methods to enhance efficiency and environmental responsibility in manufacturing processes [23]. Mia et al. devised an Artificial Neural Network (ANN)-based predictive model with a 3-17-1 architecture for surface quality in the MQL-assisted hard turning process. The mean absolute error was computed at 2.49%. Through statistical analysis, the study identified optimal process parameters [24]. Yurtkuran et al. built machine learning predictive models, such as a Gradient Boosting Machine, Linear Regression, Multilayer Perceptron, and AdaBoost Regression, to predict the energy usage during the machining of PH13-8Mo stainless steel under five different cooling conditions: pure MQL, Gnps-mixed MQL, hBN-mixed MQL, cryogenic cooling, and cryogenic cooling combined with MQL. Among these models, the Gradient Boosting Machine demonstrated the lowest error rate [25].

The Adaptive Neuro-Fuzzy Inference System (ANFIS) model, integrating fuzzy logic principles with neural network architectures, stands as a valuable approach for precise modeling of complex systems. Dambatta et al. developed an ANFIS model while machining silicon nitride ceramic material utilizing a SiO_2 nanoparticle with vegetable base oil, showcasing exceptional predictive abilities. The model demonstrated a remarkable accuracy, achieving 97.82% for grinding force prediction and 96.4% for surface roughness prediction [26]. In a related context, Gupta et al. undertook a comparative analysis between ANFIS and RSM during the cutting process of titanium alloy in a nano-MQL environment to predict machining force, cutting temperature, and surface smoothness. The study's results showcased the superior performance of ANFIS [27].

After an extensive review of the available literature, it is clear that there is a notable absence of studies examining the performance of milling operations on AISI H11 steel using Gnps-enhanced sesame oil in MQL systems. Despite the numerous benefits of sesame oil as a lubricant, such as its excellent thermal stability, high oxidative resistance, biodegradability, and its ability to reduce friction and wear, research in this area remains notably limited.

Furthermore, sesame oil offers significant health benefits compared to other vegetable oils, including its hypoallergenic properties and non-toxic nature, which make it a safer alternative in machining environments. Unlike some other vegetable oils, such as those high in polyunsaturated fats like soybean and corn oil, which can produce harmful compounds when oxidized at high temperatures, sesame oil is less likely to cause allergic reactions and is more stable under heat. This stability reduces potential health risks for operators.

The scarcity of research in this area highlights the need for further investigation to fully explore the potential advantages of sesame oil in advanced machining processes. Additionally, there is a notable lack of studies on the prediction of cutting temperatures and surface roughness in MQL machining environments using intelligent models. Few reports have utilized additional test data to validate the predictive accuracy of developed models. This limited focus underscores the novelty and significance of the proposed research endeavor. Consequently, the scope of this experimental study is to assess the impact of a Gnps-mixed sesame oil MQL system on the end milling process of AISI H11 hot die steel.

The investigation will systematically examine critical cutting parameters, including cutting speed, feed rate, cooling environment, and MQL air pressure. The study will quantify cutting temperature and surface roughness across a spectrum of machining conditions. To optimize experimental output performance, Taguchi statistical analysis will be employed. Subsequently, ANOVA will be applied to provide an in-depth analysis of the significant factors influencing cutting temperature and surface roughness. Furthermore, this study will incorporate ANFIS to predict cutting zone temperature and surface quality. Finally, the confirmatory experiments were conducted to rigorously validate the integrity and accuracy of the developed models, thereby ensuring their robustness and reliability for practical application.

2. Materials and Methods

2.1. Experimental Setup

The experiment involves using a plate of AISI H11 hot die steel, with its composition determined by optical emission spectroscopy test results, as presented in Table 1. The plate dimensions used in the experiment are 100 mm × 100 mm × 9 mm. The cutting processes are conducted on the LMW CNC vertical machining center LV 45 with a 5.5 kw power, as depicted in Figure 1. For the milling operation, a TiAlN-coated, 4-flute carbide end mill cutter with a 6 mm diameter, 30° helix angle, 20 mm flute length, and 64 mm overall length is used. Throughout the experimentation, the MQL flow rate is consistently maintained at 60 mL/h, while the air pressure varies at 2 bar, 4 bar, and 6 bar [28–30]. Two distinct cooling environments are employed in this study: pure MQL (PMQL) and Gnps-mixed MQL (GNMQL). The cutting parameters were chosen based on recommendations from the tool manufacturer and previous study [31], as detailed in Table 2. These parameters were methodically arranged for experimentation using the Taguchi L_{36} orthogonal design, as shown in Table 3. Following the successful experimentation, the optimization procedure was executed through the Taguchi Signal-to-Noise (S/N) proportion methodology, utilizing Minitab 18 software. Additionally, the development of ANFIS prediction models for the estimation of cutting temperature and surface roughness was undertaken using MATLAB 2017.

Table 1. Composition of AISI H11 in the received stage.

Element	C	Si	Mn	P	S	Cr	Mo	V	Fe
Weight %	0.4	0.98	0.25	0.021	0.01	4.88	1.21	0.42	92.19

Table 2. Machining condition.

Input	Description
Machining environments	PMQL, GNMQL
Cutting fluid	Sesame oil, Graphene-mixed sesame oil
Cutting speed	40 m/min, 50 m/min, 60 m/min
Feed rate	0.01 mm/rev, 0.02 mm/rev, 0.03 mm/rev
Depth of cut	1 mm
MQL fluid flow rate	60 mL/h
MQL jet pressure	2 bar, 4 bar, 6 bar

Table 3. Experimental design and corresponding responses.

Experiment Number	Cooling	Cutting Speed m/min	Feed Rate mm/rev	MQL Pressure Bar	Cutting Temperature °C	Surface Roughness µm
1	PMQL	40	0.01	2	63	0.286
2	PMQL	50	0.02	4	85	0.361
3	PMQL	60	0.03	6	98	0.358
4	PMQL	40	0.01	4	58	0.243
5	PMQL	50	0.02	6	92	0.376
6	PMQL	60	0.03	2	118	0.362
7	PMQL	40	0.01	6	63	0.266
8	PMQL	50	0.02	2	119	0.376
9	PMQL	60	0.03	4	94	0.298
10	PMQL	40	0.03	4	59	0.297
11	PMQL	50	0.01	2	87	0.3597
12	PMQL	60	0.02	6	106	0.425
13	PMQL	40	0.02	4	61	0.265
14	PMQL	50	0.03	6	90	0.323
15	PMQL	60	0.01	2	136	0.382
16	PMQL	40	0.02	2	72	0.275
17	PMQL	50	0.03	4	77	0.298
18	PMQL	60	0.01	6	87	0.525
19	GNMQL	40	0.02	2	64	0.322
20	GNMQL	50	0.03	4	71	0.183
21	GNMQL	60	0.01	6	58	0.172
22	GNMQL	40	0.02	4	57	0.228
23	GNMQL	50	0.03	6	82	0.293
24	GNMQL	60	0.01	2	86	0.193
25	GNMQL	40	0.03	4	55	0.286
26	GNMQL	50	0.01	6	73	0.296
27	GNMQL	60	0.02	2	98	0.361
28	GNMQL	40	0.01	6	60	0.248
29	GNMQL	50	0.02	4	80	0.196
30	GNMQL	60	0.03	2	75	0.336
31	GNMQL	40	0.03	6	58	0.251
32	GNMQL	50	0.01	2	77	0.334
33	GNMQL	60	0.02	4	82	0.241
34	GNMQL	40	0.03	2	60	0.293
35	GNMQL	50	0.01	4	70	0.274
36	GNMQL	60	0.02	6	90	0.261



Figure 1. Experimental setup.

2.2. Preparation of Gnps Nanofluid

Biodegradable sesame seed oil is employed as the base cutting oil for the GNMQL system, given its exceptional lubrication, widespread cultivation, and economic viability. Furthermore, it aligns with environmental consciousness owing to its biodegradable properties [9,14]. The Gnps, obtained from the market, were incorporated as an additive in sesame-based oil. The Gnps specifications provided by the supplier are as follows: thickness 5–10 nm, length 5–10 µm, density 0.279 g/cm^3, surface area 200–240 m^2/g, number of layers 4–10, and thermal conductivity 2000 W/m-K. The Gnps are characterized through the examination using a Scanning Electron Microscope (SEM) and X-Ray Diffraction (XRD), as depicted in Figure 2. The XRD analysis shows a significant peak near 26.5° 2θ, which corresponds to the (002) plane of graphitic carbon. This peak confirms the presence of graphene and indicates the typical interlayer spacing found in graphene and graphite [32]. Examination of the SEM image reveals that the graphene forms a sheet-like structure with noticeable folds, wrinkles, and overlapping layers. These characteristics reflect the underlying grain structure. The crumpled and folded appearance of the sheets enhances their mechanical flexibility and strength. Furthermore, the well-defined sheet morphology and smooth surface suggest a high degree of crystalline quality in the graphene [33].

The selected concentration of Gnps in the base oil is 0.8 wt.%, in accordance with the literature [18]. To ensure a thorough and consistent amalgamation, the mixture underwent a 30 min ultrasonication process in a Lark ultrasonic bath [34]. This step was crucial for achieving uniform mixing. Subsequently, the blended mixture was subjected to a magnetic stirrer operating at a speed of 600 rpm for duration of 45 min. This phase was implemented to enhance the homogeneity of the process.

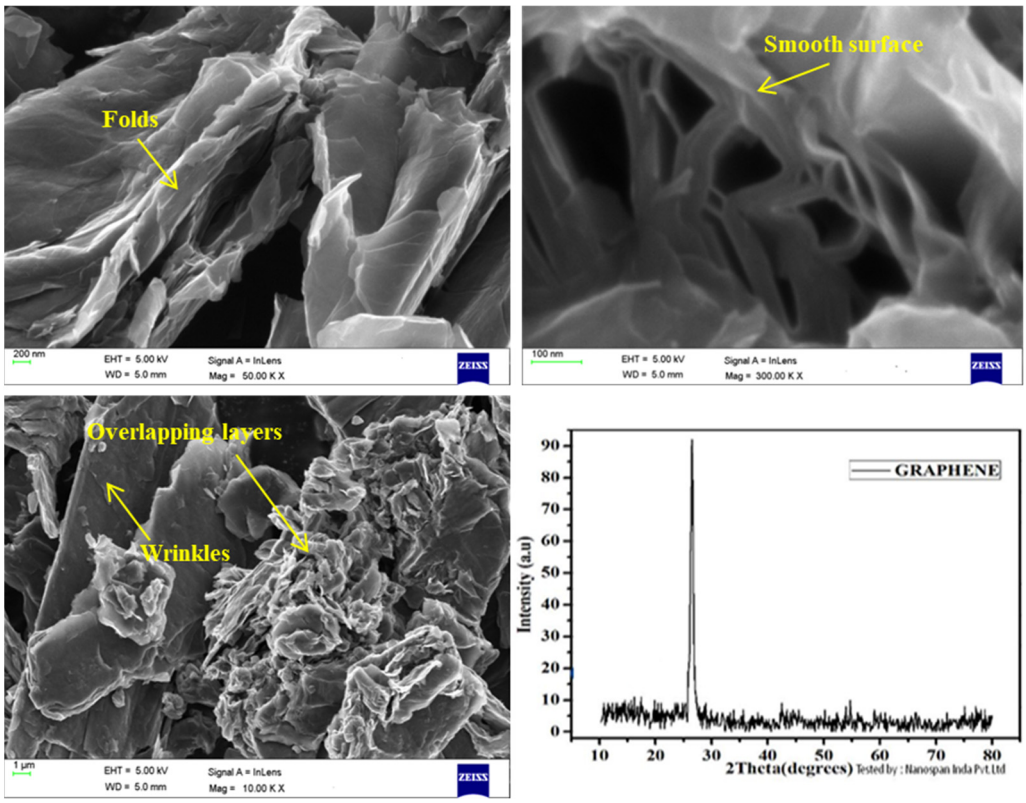

Figure 2. SEM and XRD images of Gnps.

2.3. Measurement of Responses

The temperatures in the cutting area were measured using a Taplan-coated K-type thermocouple, known for its ability to gauge temperatures up to 1260 °C. This thermocouple was seamlessly integrated with an National Instrument DAQ 9212 data acquisition system, ensuring comprehensive data capture. The thermocouples are embedded in pre-drilled holes within the workpiece to monitor cutting temperature. To enhance measurement accuracy, a 0.5 mm gap is provided between the machined surface and the thermocouple tip. A heat transfer paste with thermal conductivity exceeding 1.93 W/m-K is applied to fill the narrow space between the thermocouple wire and the workpiece. The separation between the thermocouple's sensing element and the machining surface is uniformly set at 0.5 mm to ensure precision in temperature measurement. In addition, any tiny space between the workpiece and the thermocouple wire is sealed with heat transfer paste, enhancing thermal conductivity and minimizing heat loss during the measurement [35]. The thermocouple outputs are captured by the highly sensitive NI DAQ 9212 computerized compact data acquisition system. Identified potential causes of error in the temperature assessment process using the NI DAQ system encompass deviations such as inadequate proximity of thermocouples to the machining area, improper choice of thermocouple model, and the risk of overlooking swift temperature fluctuations due to a sluggish data acquisition rate [36]. To obviate the aforementioned sources of error, a series of exacting measures have been implemented. Thermocouples are positioned at four distinct locations within drilled holes located at the base of the workpiece.

To facilitate effective data capture, the NI DAQ 9212 data acquisition system is configured to record data at a rate of 96 samples per second for each channel [31]. Moreover, the FLIR E60 infrared thermal imaging camera is employed as a supplementary tool to enhance the accuracy of data acquisition by enabling cross-verification throughout the temperature evaluation process. This advanced camera system captures thermal images at five distinct

intervals during each cutting stroke, thus providing an additional layer of validation [37]. For streamlined data analysis and interpretation, the highest observed temperature values are selectively chosen from the NI DAQ system's dataset for every end mill cutting process. This process entails iteration through the captured data stored within the system's buffer, ensuring comprehensive evaluation of temperature dynamics.

The determinant for validating the operational efficacy of machining lies in the precise measurement of surface roughness values. In accordance with ISO 21920-2:2021 standards [38], surface assessment relies on the Ra parameter [39]. To meet this requirement, a well-defined protocol is followed, which includes specific parameters, a 5 mm sample length, 0.8 mm cut-off length, a scanning speed of 0.5 mm/s, and a sample size of 5 [40], was adhered to during the surface roughness measurement process using the Mitutoyo SJ 401 device. Moreover, an SEM was utilized to analyze the surface topography of the machined surface of the confirmatory experiment.

3. Results and Discussions

3.1. Influence of Machining Conditions on Cutting Temperature

Elevated cutting temperatures and heightened friction within the cutting region represent the primary catalysts for both tool wear and excessive surface roughness in the machining domain. In the course of the milling process, a substantial proportion of the mechanical energy undergoes conversion into heat. This augmented heat, in turn, induces thermal impairment to the cutting tool as well as workpiece [41]. The impact of machining conditions on cutting temperature under a PMQL environment is elucidated in Figure 3. Figure 3a shows the impact of cutting speed at three distinct jet pressures on cutting temperature. Notably, the cutting region temperature escalates with the augmentation of cutting speed, attributable to heightened friction in the tool–chip interaction [42].

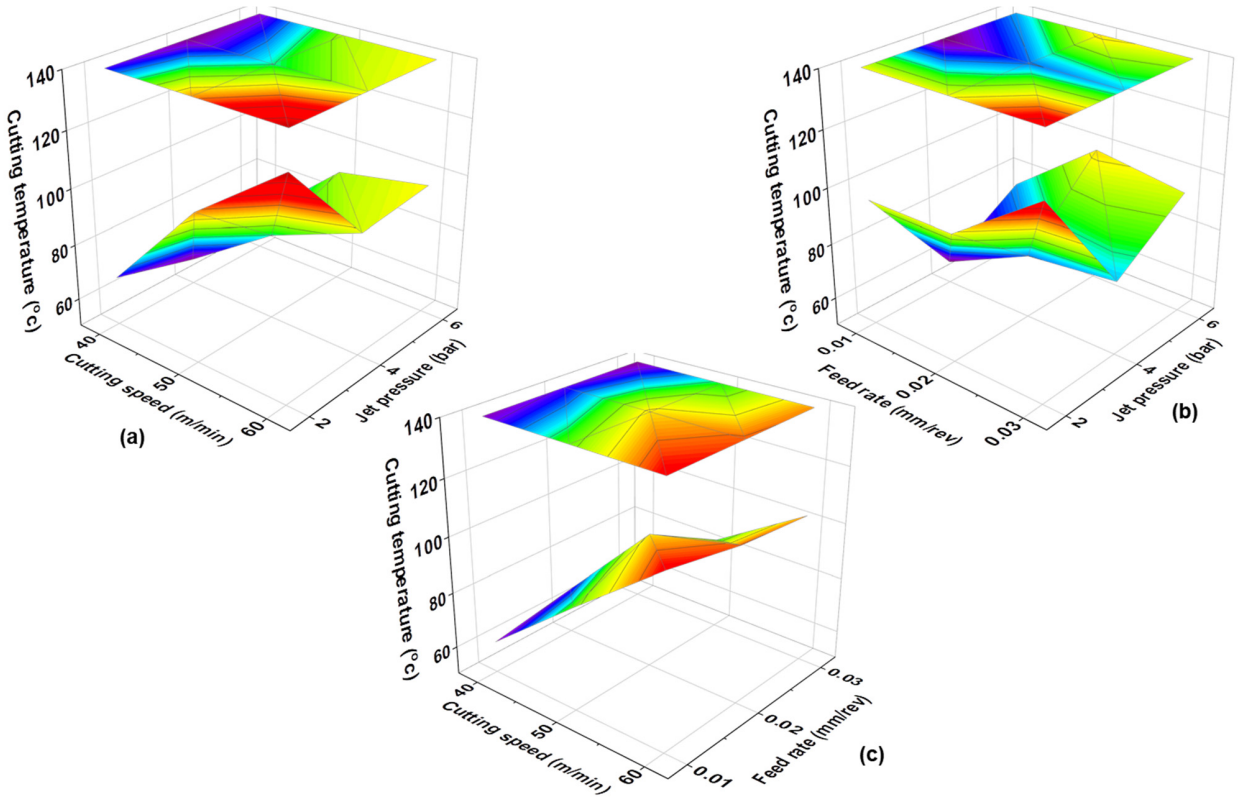

Figure 3. Cutting temperature at PMQL environment (**a**) cutting speed vs. jet pressure, (**b**) feed rate vs. jet pressure, and (**c**) cutting speed vs. feed rate.

An efficient decrease in cutting temperature is achieved with an elevation in jet pressure, reaching optimal efficacy at 4 bar pressure. This reduction is attributed to the augmented pressure providing a heightened lubrication effect within the cutting region, facilitated by the production of small-diameter droplets of oil mist under higher air pressure. These droplets exhibit superior penetration capability in contact zones [43], a phenomenon corroborated by Sadeghi et al. while machining titanium alloy by surface grinding with vegetable-based oil [44]. The reduction in temperature remains effective until a 6 bar pressure threshold, beyond which a temperature increase is observed. This temperature surge is attributed to excessively high air pressure inducing a spring-back effect of droplets from the cutting surface, resulting in an ineffective lubrication process [45].

Figure 3b illustrates that the highest cutting temperature is observed at a higher feed rate combined with a lower MQL pressure, whereas the lowest cutting temperature occurs at the lowest feed rate with medium MQL pressure. At lower feed rates, a moderate MQL pressure provides optimal cooling and lubrication for reducing friction and heat generation. In contrast, higher feed rates increase material deformation and friction, leading to higher temperatures, especially when MQL pressure is insufficient to provide adequate cooling and lubrication [46]. Figure 3c elucidates the correlation of cutting temperature under various cutting speeds and feed rate conditions. The surface graph reveals that lower cutting speeds and feed rates correspond to lower cutting temperatures, while higher cutting speeds and feed rates result in elevated cutting temperatures. This phenomenon is attributed to the slower movement in low-cutting speed and feed rate conditions, allowing the coolant to more effectively reach the cutting zone. Conversely, at higher cutting speeds and feed rates, the coolant fails to reach the cutting zone adequately, contributing to increased cutting temperatures [47]. A comparable observation was made by Binali et al. during the milling of Nimaxm under the olive oil-based MQL condition [48]. The temperatures in the cutting zone were promptly recorded under all parametric conditions using a thermal camera, as shown in Figure 4.

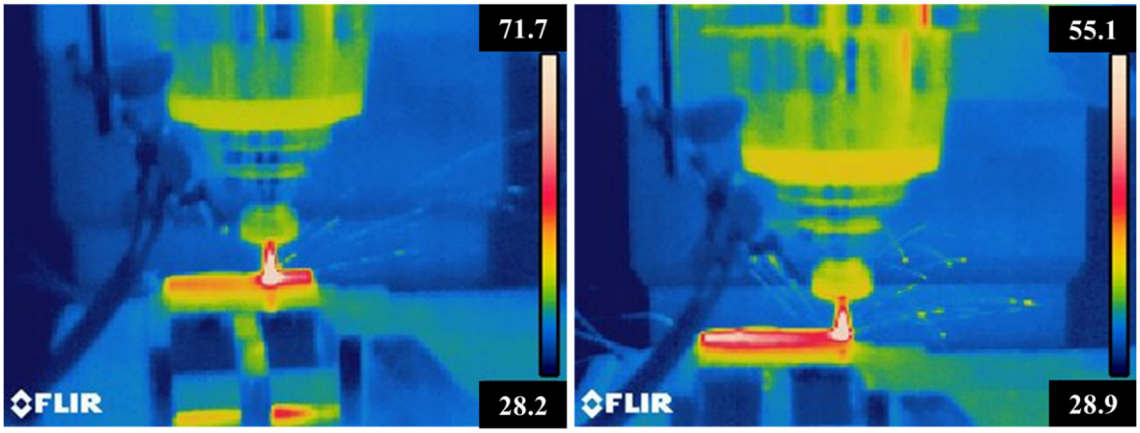

Figure 4. FLIR images at PMQL and GNMQL conditions.

The integration of Gnps into MQL cutting fluids offers a trifecta of benefits for machining. Exceptional thermal conductivity acts as a shield against heat generation, leading to reduced tool wear and minimized workpiece distortion [49]. Figure 5 depicts the effect of machining conditions on cutting temperature under GNMQL cooling conditions. In Figure 5a, a substantial reduction in cutting temperature is evident across all cutting speed and pressure conditions compared to PMQL environments. This reduction is attributed to the rapid heat propagation facilitated by the exceptional thermal diffusivity property of Gnps in the GNMQL environment [50].

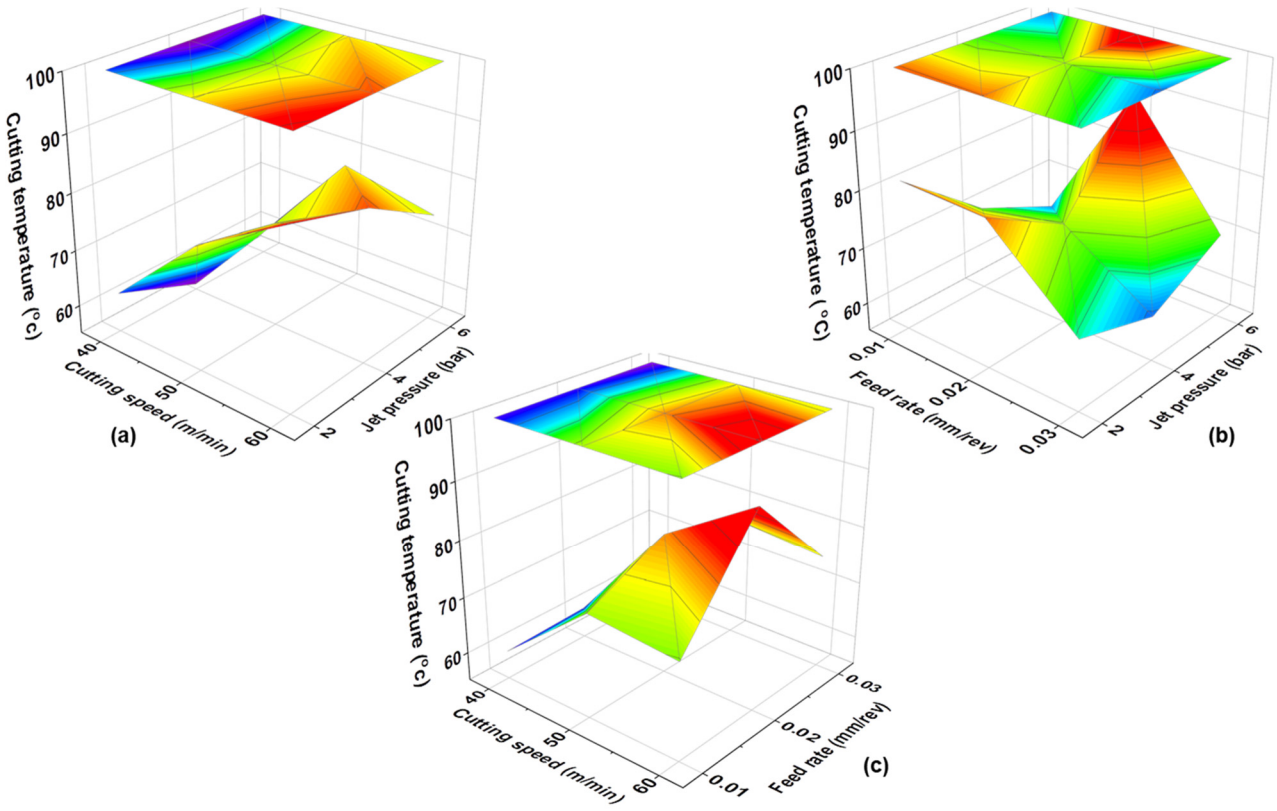

Figure 5. Cutting temperature at GNMQL environment (**a**) cutting speed vs. jet pressure, (**b**) feed rate vs. jet pressure, and (**c**) cutting speed vs. feed rate.

The influence of cutting temperature concerning feed rate and jet pressure is depicted in Figure 5b. The lowest temperature of 55 °C is reached at a 0.03 mm/rev feed rate, 4 bar pressure, and 40 m/min cutting speed. This represents a significant reduction from the same parametric conditions in PMQL environments. A similar reduction phenomenon was reported by Li et al. while a titanium alloy is being machined in Gnps-mixed vegetable oil MQL circumstances [51]. The lower temperature value recorded in high pressure and low pressure regions was compared to the PMQL environment. The limitations of suboptimal lubrication in the PMQL environment, caused by poor atomization at low pressure and disruption of the lubrication film at high pressure, can be mitigated. This improvement stems from the nanoparticles' ability to enhance the fluid's dispersion, stability, and viscosity, enabling better atomization at lower pressures and maintaining a consistent film at higher pressures [52].

As illustrated in Figure 5c, it is recognized that the drawback of inadequate coolant supply at higher cutting speeds and feed rates in PMQL environments is significantly minimized in GNMQL environments. This enhancement is credited to the Brownian motion of Gnps, characterized by random movement resulting from collisions with adjacent molecules. This phenomenon guarantees extensive coverage of the lubricating fluid across the cutting zone, thereby facilitating efficient heat dissipation [53]. Analysis of the surface graphs reveals that the lowest cutting temperature of 55 °C was achieved under optimal machining conditions: a GNMQL environment, a cutting speed of 40 m/min, a feed rate of 0.03 mm/rev, and an MQL jet pressure of 4 bar.

3.2. Influence of Machining Conditions on Surface Roughness

The performance of a workpiece, with regard to its mechanical properties and service life, is significantly impacted by its surface quality. Figure 6 illustrates the effect of cutting

parameters on surface smoothness in the PMQL environment. The surface quality improves as cutting speed increases up to a 4 bar pressure region. This phenomenon can be attributed to improved chip evacuation and efficient heat dissipation within a shorter contact time, thus preventing thermal damage to the surface [54]. Significantly, surface roughness values exhibit a lower trend in the 4 bar pressure regions in contrast to the 2 bar pressure region. A comparable effect was observed by Rohit et al. during the milling of SS304 steel under the LRT 30 biodegradable ester cutting oil-based MQL environment [29]. However, in the 6 bar pressure region, there is a slight increase in roughness compared to the 4 bar region. This occurrence is linked to the ineffectiveness of the atomization process at low pressure, resulting in poor lubrication and cooling effects, leading to higher friction, temperature, and consequently, higher surface roughness values. Excessive pressure, on the other hand, may wash away the lubricant from the milling zone, increasing resistance and temperature and negatively impacting surface finish [55].

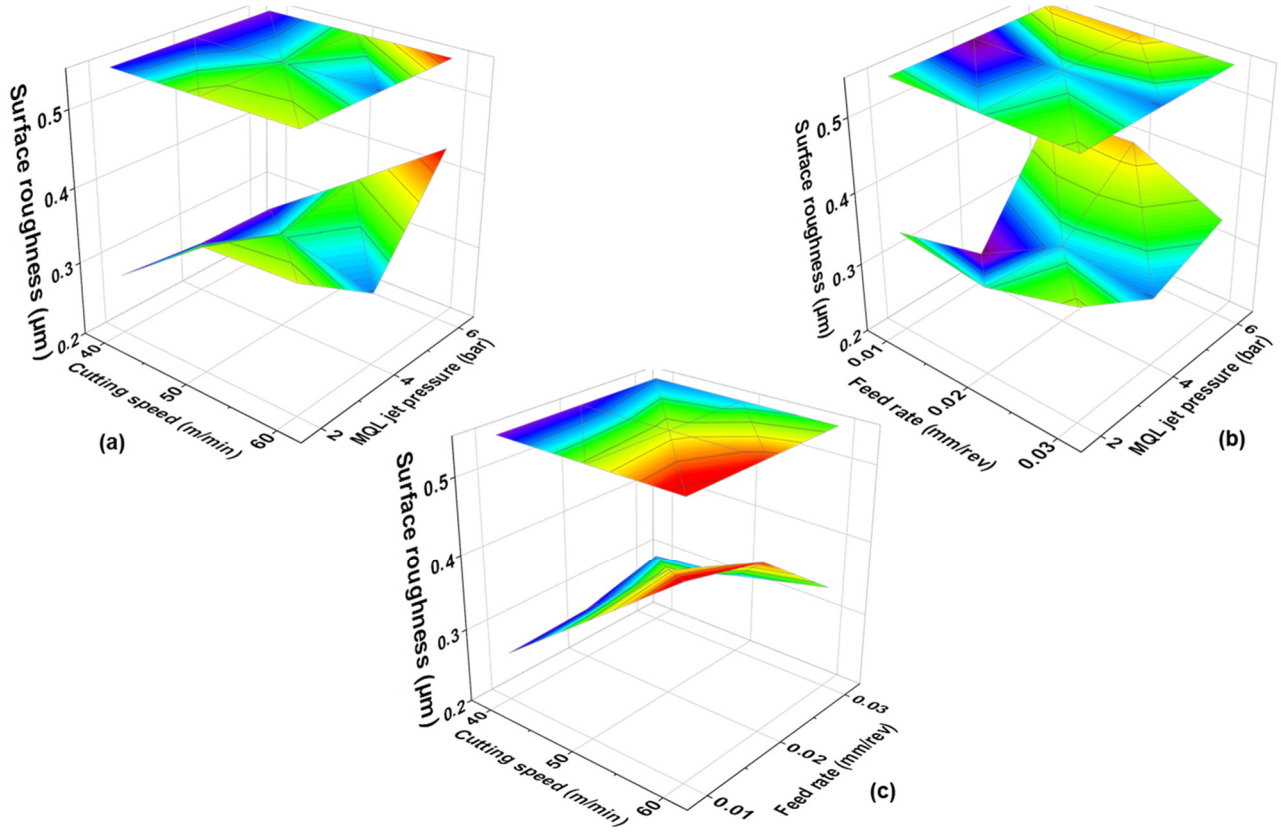

Figure 6. Surface roughness at PMQL environment (**a**) cutting speed vs. jet pressure, (**b**) feed rate vs. jet pressure, and (**c**) cutting speed vs. feed rate.

Higher surface roughness values are observed at all feed rate values when the MQL pressure is 6 bar. This is attributed to ineffective chip evacuation, leading to scratches and re-cutting. Optimal surface quality is achieved at reduced feed rates and cutting speeds, minimizing the generation of built-up edge on the cutter [56]. Conversely, higher cutting speeds and feed rates result in elevated surface roughness due to inconsistent cutting forces caused by tool deflection and vibration [57].

Figure 7 presents the surface roughness variations in different cutting conditions within the GNMQL environment. The introduction of spherical-shaped nanoparticles between the milling cutter and workpiece facilitated a rolling action, substantially reducing resistance, wear, and heat generation during cutting operations. Consequently, this resulted in lower surface roughness values across all cutting speed conditions compared to the

traditional PMQL environment. Notably, a higher surface roughness value was recorded in the 2 bar pressure region, indicating insufficient flow and dispersion of the nanofluid due to agglomeration [58]. This phenomenon adversely affected surface quality.

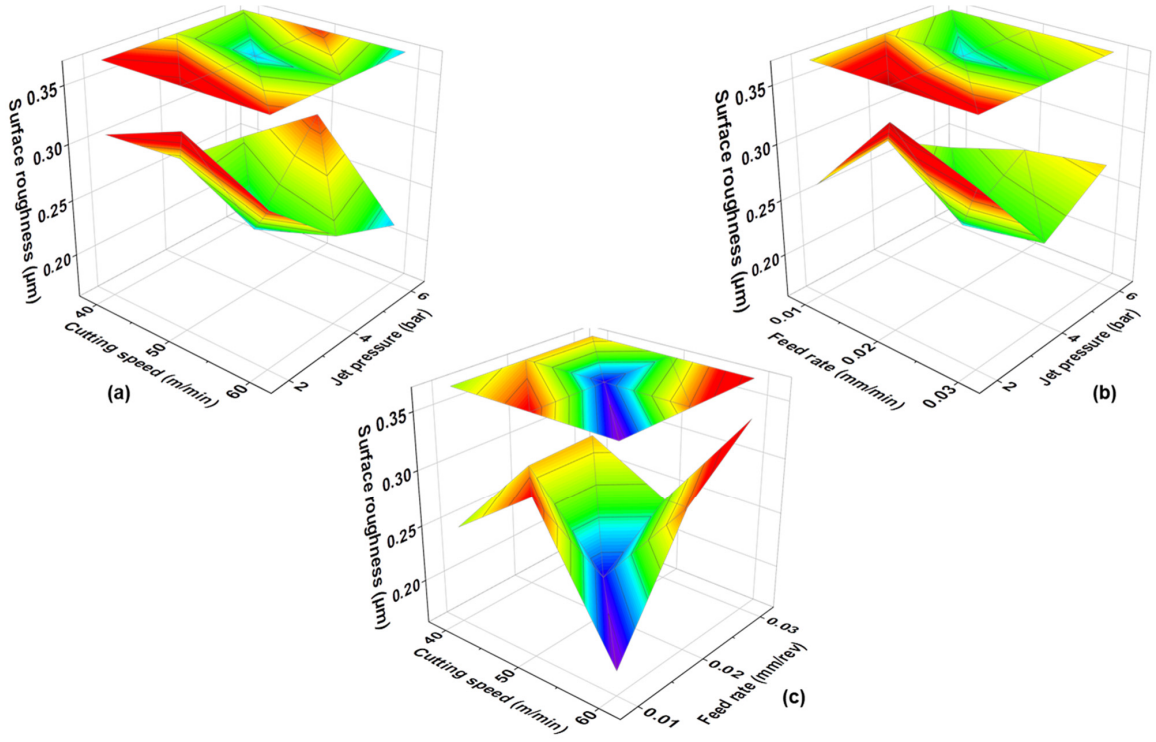

Figure 7. Surface roughness at GNMQL environment (**a**) cutting speed vs. jet pressure, (**b**) feed rate vs. jet pressure, and (**c**) cutting speed vs. feed rate.

The minimum surface roughness was recorded at a 0.01 mm/min feed rate level and a higher pressure range. This can be ascribed to the lower feed rate allowing the lubricating fluid and nanoparticles to penetrate deeper into the convergence of the cutter and workpiece. Additionally, the higher pressure reduces nanoparticle agglomeration, enhancing dispersion, cooling, and lubrication [59]. The nanoparticles, through their polishing activities, removed burrs and ridges, resulting in a refined surface finish [60]. Lower surface finish was observed at lower machining parameter conditions and vice versa. The enhancement in surface quality is due to the polishing and self-repairing effects enabled by the nanoparticles. The nanoparticles' abrasive effect in the cutting fluid reduces surface irregularities and micro-defects on the machined surface [61], while their ability to fill minor voids in the workpiece or cutting tool contributes to an overall improvement in surface quality [62]. Thus, the lowest surface roughness of 0.172 µm was achieved with optimal machining conditions, which included a GNMQL environment, a cutting speed of 60 m/min, a feed rate of 0.01 mm/rev, and an MQL jet pressure of 6 bar.

3.3. Taguchi-Based Analysis of Optimum Parameters

The optimal parametric combination for the end milling process was determined using the Taguchi Signal-to-Noise (S/N) ratio, a statistical measure that helps identify the settings for controllable factors (signals) that minimize unwanted variability caused by uncontrollable factors (noise). The experimental factors and their corresponding levels are summarized in Table 4. A mixed-level design was selected within the framework of Taguchi's method. The response variables for the two statistical analyses were milling temperature and surface roughness, corresponding to the specified factor levels. To improve

machining performance, both response variables were targeted for a "smaller-the-better" characteristic.

Table 4. Statistical analysis factors and levels.

Symbol	Factors	Level		
		1	**2**	**3**
A	Cooling condition	PMQL	GNMQL	
B	Cutting speed (m/min)	40	50	60
C	Feed rate (mm/rev)	0.01	0.02	0.03
D	MQL jet pressure (bar)	2	4	6

The optimal end milling process parameters for achieving improved cutting temperature are identified with a GNMQL cooling environment at a cutting speed of 40 m/min, feed rate of 0.01 mm/rev, and 4 bar MQL jet pressure (Figure 8). The optimum parameters for enhancing surface quality are identified with a GNMQL cooling environment at a cutting speed of 40 m/min, feed rate of 0.01 mm/rev, and 4 bar MQL jet pressure (Figure 9). These findings contribute to refining the overall effectiveness of the milling process.

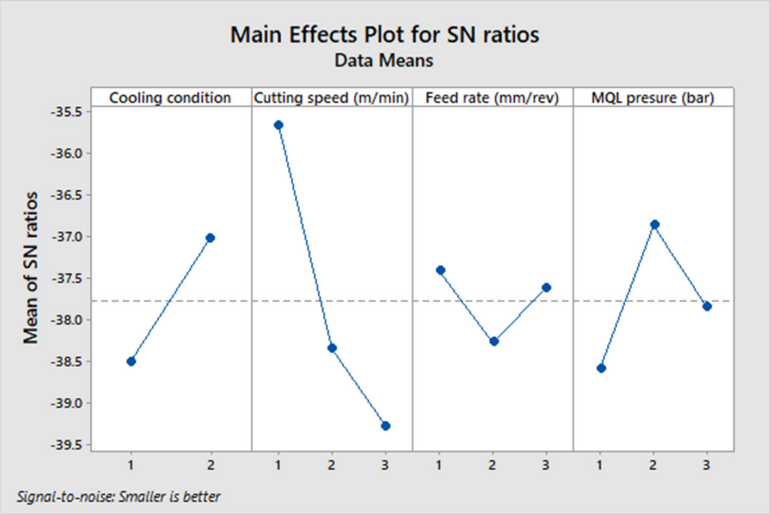

Figure 8. Effect of process variables on cutting temperature.

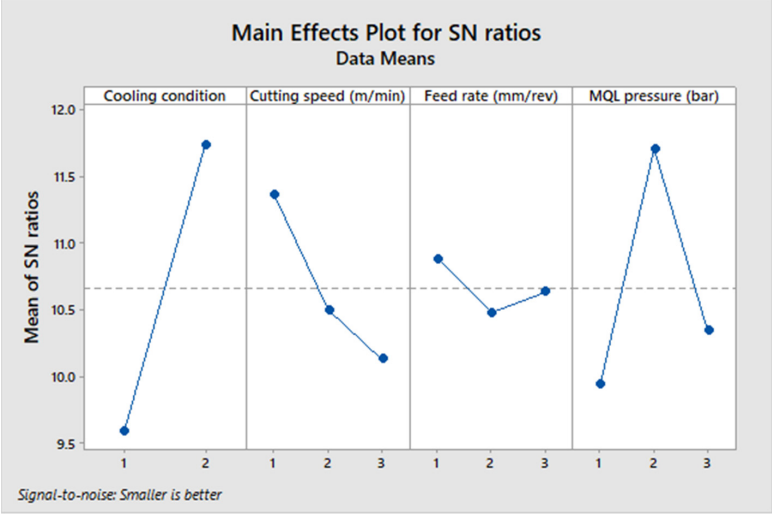

Figure 9. Effect of process variables on surface roughness.

The mean values resulting from the statistical analysis of cutting temperature and surface roughness are presented in Tables 5 and 6, respectively. The cutting speed exerts the predominant influence on cutting temperature, followed by MQL jet pressure, with the cooling condition exhibiting a comparatively lower impact. Notably, the feed rate emerges as the least influential parameter affecting the cutting temperature. The hierarchical order of influence of milling factors on cutting temperature is established as cutting speed (B) > MQL jet pressure (D) > cooling condition (A) > feed rate (C). Conversely, the least impactful factors for surface smoothness are cooling condition and feed rate. The order of influence for each parameter is determined as cooling condition (A) > MQL jet pressure (D) > cutting speed (B) > feed rate (C).

Table 5. Mean value of cutting temperature.

Level	A	B	C	D
1	86.94	60.83	76.50	87.92
2	72.00	83.58	83.83	70.75
3		94.00	78.08	79.75
Delta	14.94	33.17	7.33	17.17
Rank	3	1	4	2

Table 6. Mean value of surface roughness.

Level	A	B	C	D
1	0.3375	0.2717	0.2982	0.3233
2	0.2649	0.3058	0.3073	0.2642
3		0.3262	0.2982	0.3162
Delta	0.0726	0.0545	0.0091	0.0591
Rank	1	3	4	2

3.4. Analysis of Variance

The Analysis of Variance (ANOVA) was employed to assess the statistical significance of process parameters on machinability characteristics, as presented in Table 7. This table includes the F-ratio, a key indicator used to identify the control factors that significantly affect the characteristic under investigation. The analysis was conducted at a 5% significance level, corresponding to a 95% confidence level [63]. The ANOVA results for cutting temperature indicate that cutting speed is the most significant factor, accounting for 70.779% of the variation with a substantial F-ratio of 348.374. MQL jet pressure also plays a critical role, contributing 14.909% to the variation with an F-ratio of 73.387. The cooling condition, while significant with a contribution of 7.433% and an F-ratio of 73.172, has a relatively moderate impact compared to cutting speed. The feed rate has the least influence, contributing only 4.034% with an F-ratio of 19.855.

Table 7. ANOVA for cutting temperature and surface roughness.

Factors	Degree of Freedom	Sum of Squares	Mean of Squares	F-Ratio	Percentage Contribution
(a) Cutting temperature					
Cooling condition	1	2.223	2.223	73.172	7.433
Cutting speed	2	21.163	10.582	348.374	70.779
Feed rate	2	1.206	0.603	19.855	4.034
MQL jet pressure	2	4.458	2.229	73.387	14.909
Error	28	0.85	0.03		2.844
Total		29.901	15.667		
(b) Surface roughness					
Cooling condition	1	4.578	4.578	144.498	34.608
Cutting speed	2	2.377	1.189	37.517	17.971
Feed rate	2	0.244	0.122	3.849	1.844
MQL jet pressure	2	5.142	2.571	81.146	38.87
Error	28	0.887	0.0317		6.706
Total		13.229	8.492		

In the ANOVA analysis of surface roughness, MQL jet pressure emerges as the most significant factor, accounting for 38.87% of the variation and showing a substantial F-ratio of 81.146. The cooling condition also plays a key role, contributing 34.608% to the variation with an F-ratio of 144.498. Cutting speed, while influential, contributes 17.971% with an F-ratio of 37.517, indicating a lesser impact than MQL jet pressure and the cooling condition. The feed rate has the least impact on surface roughness, contributing only 1.844% with an F-ratio of 3.849.

3.5. Prediction of Output Performance Variables by ANFIS

In the domain of Artificial Intelligence, the ANFIS stands as a hybrid computational model, synergizing the advantages of both the ANN and fuzzy logic systems [64]. ANFIS comprises four pivotal components essential for precision in prediction—Fuzzy If-Then rules used to define the relationship between input (dependent) and output (independent) variables, membership functions for the fuzzification of independent variables, a Rule-Based Inference System utilizing AND, OR operators, and a Learning Algorithm implementing a hybrid technique with gradient descent and least square estimation [65]. The structural design of the ANFIS model comprises five layers, organized as a feed forward neural network, as illustrated in Figure 10. The stratum of the established ANFIS model encompasses various nodes, each delineated as follows:

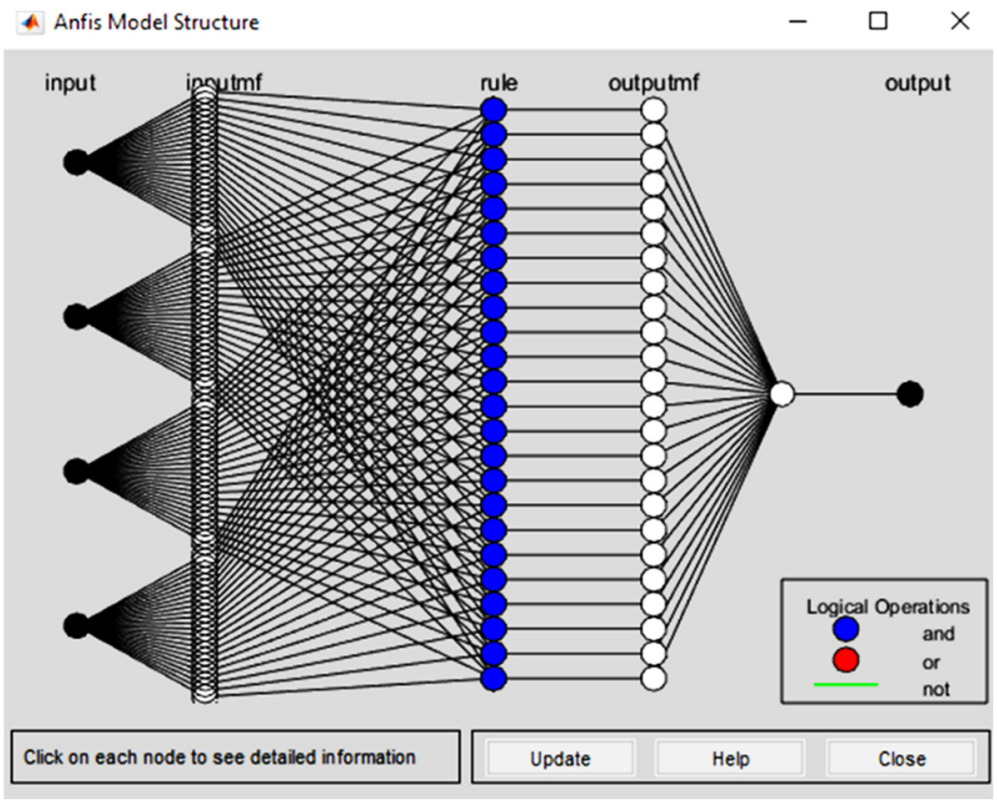

Figure 10. ANFIS model structure from MATLAB.

In the first layer, each node is indicative of a membership function corresponding to the inputs. Fuzzy values are derived from the inputs through the processing of these membership functions. The outputs of the nodes are articulated as follows:

$$O_{1,i} = \mu_{Mi}\,(a);\ i = 1,2 \tag{1}$$

$$O_{1,j} = \mu_{Nj}\,(b);\ j = 1,2 \tag{2}$$

From the above equations, $O_{1,i}$ and $O_{1,j}$ denote the output of the nodes and $\mu_{Mi}(a)$ and $\mu_{Ni}(b)$ represent the membership functions. The equations for Gaussian membership functions are as follows, with the antecedent parameters denoted as c and d.

$$\mu_{mi}(a) = e^{-\frac{1}{2}\left(\frac{a-c}{d}\right)^2} \tag{3}$$

Fixed nodes are present in the second layer of the ANFIS architecture. The fuzzy logic inference system is employed to generate rules, and the corresponding equation is presented below.

$$O_{2i} = w_i = \mu_{Mi}(a) * \mu_{Ni}(b);\ i = 1,2 \tag{4}$$

The normalization process of data is executed in the third layer, and the equation for normalization is expressed as follows:

$$O_{3i} = \overline{w}_i = \frac{w_i}{w_1 + w_2}; i = 1,2 \tag{5}$$

First-order polynomials are generated in the fourth nodes, identified as adaptive nodes. The function of the adaptive nodes is articulated as follows and the consequent parameters are represented as x_i, y_i, and z_i.

$$O_{4i} = \overline{w_i} * f_i = \overline{w_i} * (x_i a + y_i b + z_i) i = 1,2 \tag{6}$$

The de-fuzzification of normalized variables is executed in the single node of the last layer. The mathematical representation of this layer is provided below:

$$O_{5i} = \frac{\sum_i \overline{w_i} g_i}{\sum_i \overline{w_i}} \tag{7}$$

The experimental data served as the training variables for the developed ANFIS model. In training the model, 24 experimental trials were employed out of the total 36 trials, with the remaining 12 trials reserved for testing. The frequency distribution plots for all independent and dependent variables utilized during the training and validation phases are shown in Figures 11 and 12. These plots reveal that the machining environment, cutting speed, feed rate, and MQL pressure are evenly distributed across both the training and testing datasets. The skewness is present in the cutting temperature and surface roughness across both datasets. This skewness results from the data being gathered under two distinct cooling environments: PMQL and GNMQL.

The arrangement of the ANFIS model was established using MATLAB R2017a. The membership functions were tailored to facilitate the training of the model. The choice of a Sugeno-type Fuzzy Inference System (FIS) for this model was deliberate, given its advantages in terms of efficient training through gradient-based optimization, simplified parameter tuning, and interpretability with linear rule bases [66]. The FIS comprises four inputs, namely cooling condition, cutting speed, feed rate, and MQL jet pressure.

The grid partition method was employed to generate optimized rules from a provided training dataset. This method was selected for its ability to produce a transparent and interpretable model, handle computational complexity efficiently, and mitigate overfitting risks through a concise rule base [67]. The resulting information for the developed ANFIS model includes 137 nodes, 270 linear parameters, 33 nonlinear parameters, and 54 fuzzy rules. The stage of fuzzy logic design in the ANFIS model is illustrated in Figure 13. The training process involved 24 training datasets, with the final evaluation conducted on 12 testing datasets. The prediction error experienced a 100-iteration reduction, referred to as epochs, during the training and testing of the dataset, as illustrated in Figures 14 and 15.

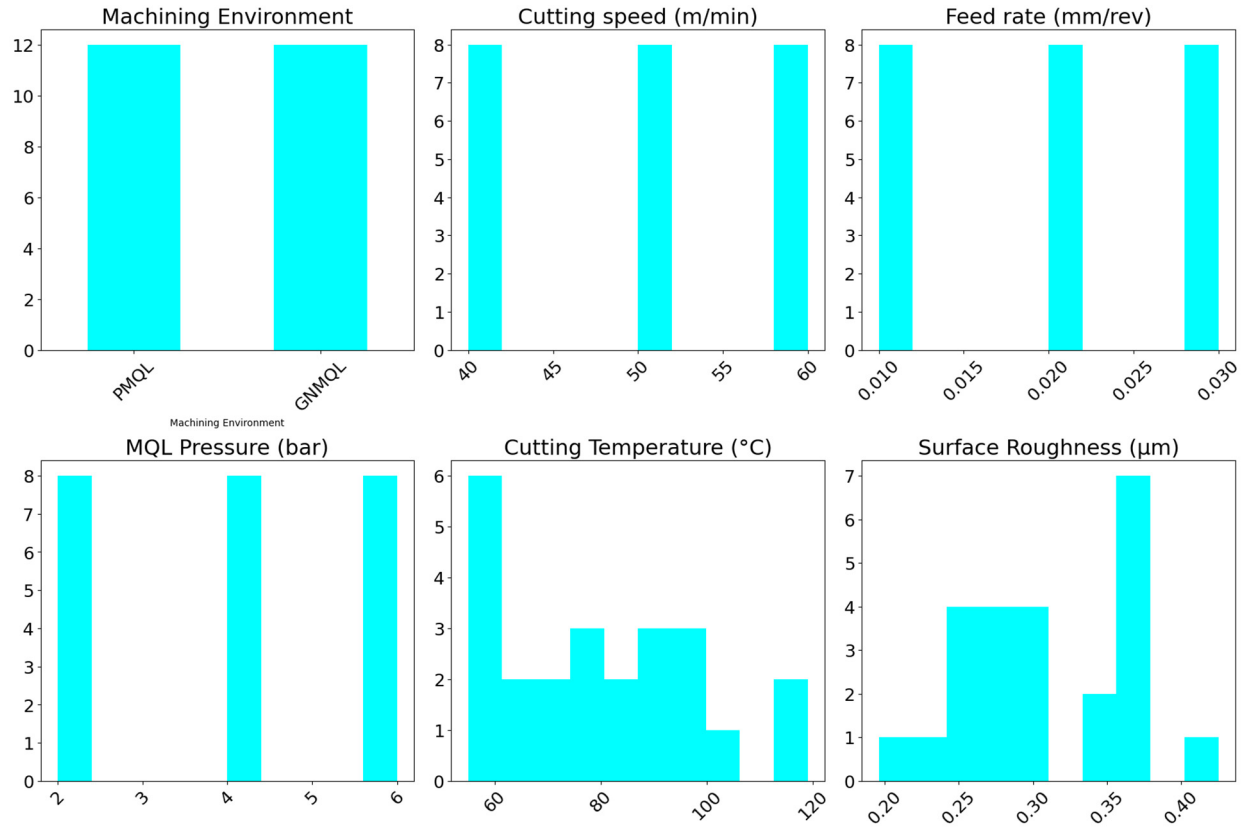

Figure 11. Distribution plot for training data.

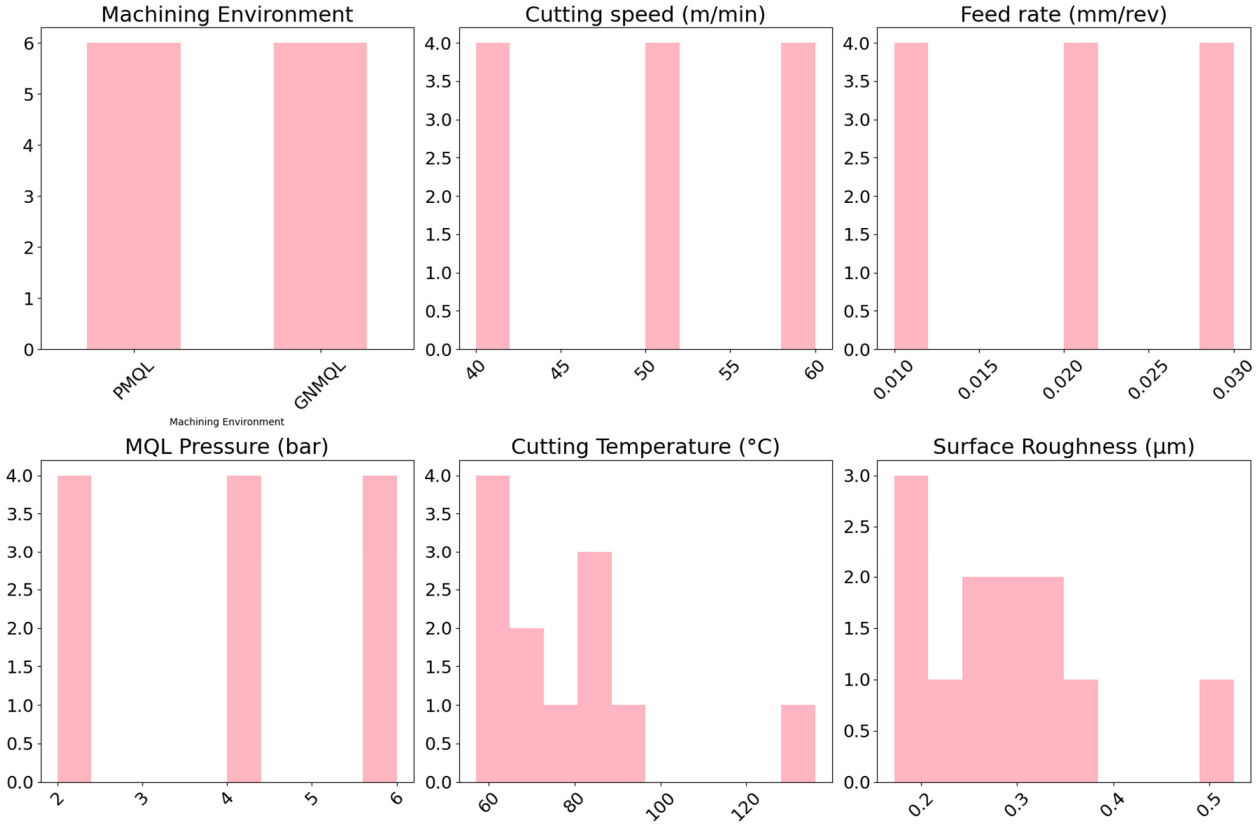

Figure 12. Distribution plot for testing data.

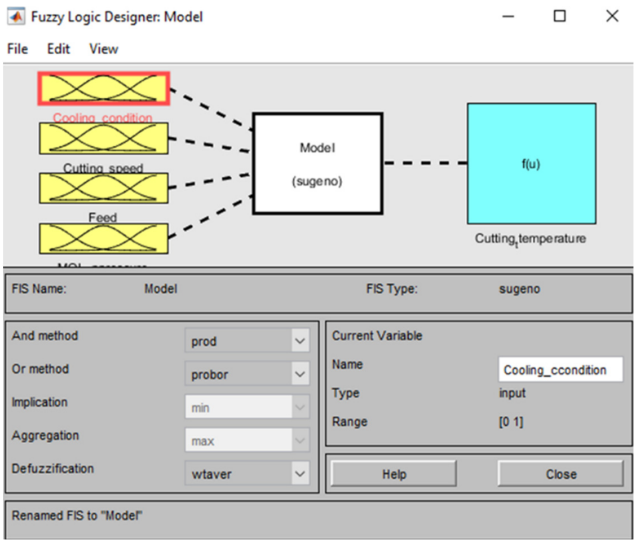

Figure 13. ANFIS model fuzzy logic designer.

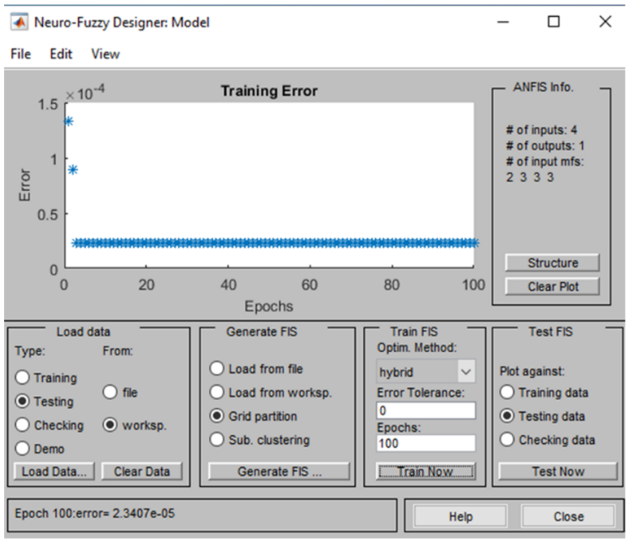

Figure 14. Training FIS of the model.

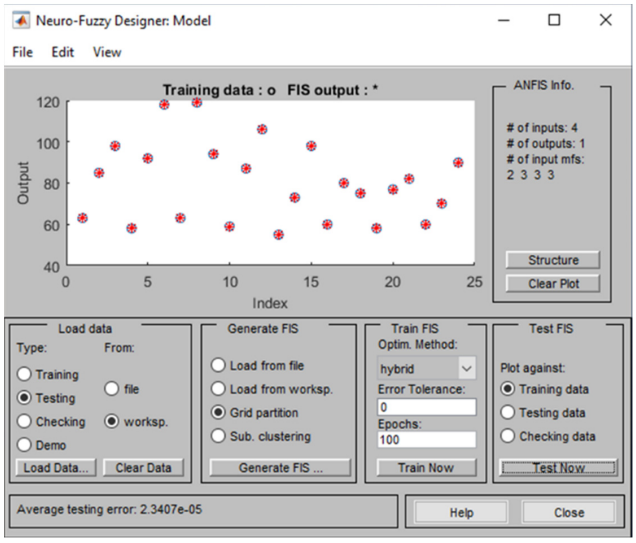

Figure 15. Testing FIS of the model.

To enhance the model's accuracy, both the training and testing of the ANFIS model were executed using various types of membership functions. The gbell membership function was specifically chosen over others due to its lower Root Mean Square Error (RMSE) of 2.3407 $\times$ 10^{-5} for the cutting temperature model and 2.005 $\times$ 10^{-7} for the surface roughness model. This optimal performance was achieved by utilizing 2, 3, 3, 3 input membership functions in the model. The comparison between experimental values versus predicted training data and experimental values versus predicted test data under the same working conditions for cutting temperature and surface roughness is presented in Figures 16 and 17. The models, distinguished by their high accuracy, yielded calculated values of 97.4% for the cutting temperature and 92.6% for surface roughness.

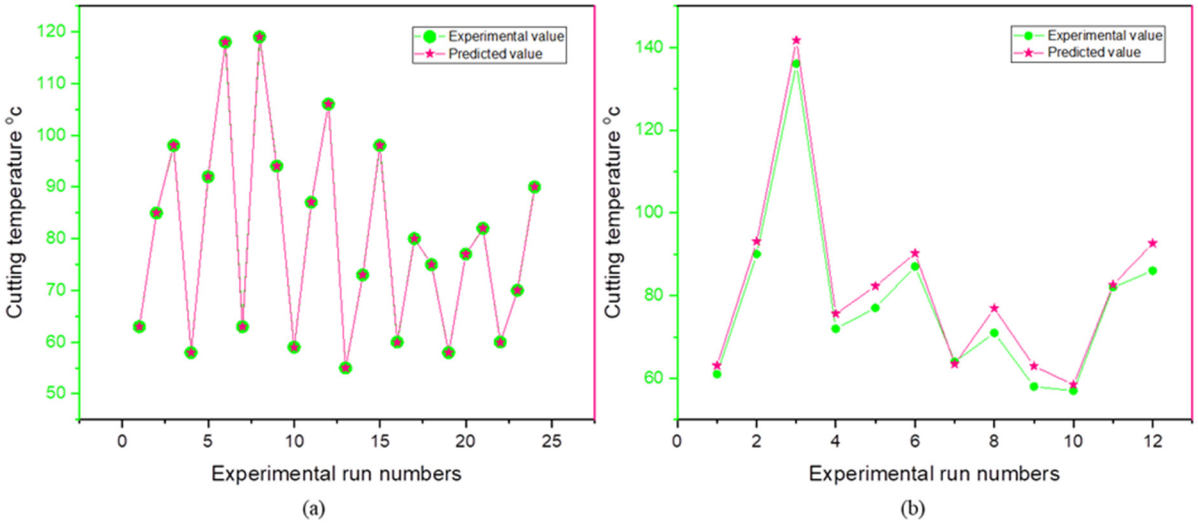

Figure 16. Observed and predicted cutting temperature (**a**) training and (**b**) testing.

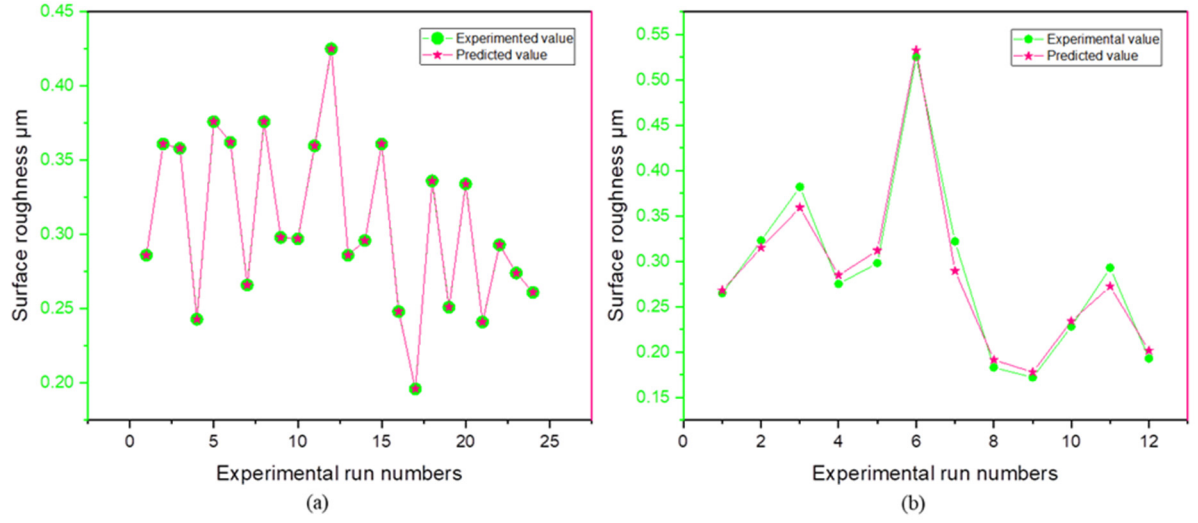

Figure 17. Observed and predicted surface roughness (**a**) training and (**b**) testing.

3.6. Confirmatory Experiments

The confirmatory milling experiments were conducted to verify the improvements achieved through Taguchi analysis. According to the Taguchi analysis, the optimal parameters for attaining reduced milling temperature and enhanced surface quality were identified as A2-B1-C1-D2. Subsequently, the cutting zone temperature and surface roughness values were predicted using the developed ANFIS model for the aforementioned optimal parameters. The confirmatory experiments were carried out under an optimal GNMQL cooling

environment with a milling speed of 40 m/min, feed rate of 0.01 mm/rev, and 4 bar MQL jet pressure. Both the predicted values from the ANFIS model and the experimental values for cutting temperature and surface roughness are presented in Table 8.

Table 8. Confirmation test compared with ANFIS predicted value.

Output Responses	Process Parameters	Predicted Value by ANFIS Model	Experimental Value	Difference
Cutting temperature, °C	A2-B1-C1-D2	52.8	51	1.8
Surface roughness, µm	A2-B1-C1-D2	0.153	0.165	0.012

SEM analysis of the machined surface was conducted for a random experiment trial starting from initial parameters and the Taguchi-forecasted optimal milling conditions. In Figure 18a, the surface resulting from machining under a PMQL cooling environment with a milling speed of 50 m/min, feed rate of 0.02 mm/rev, and 2 bar MQL pressure is depicted. The SEM image clearly reveals an abundance of scratch marks on the surface. This occurrence is ascribed to the friction and heat generated by the specified speed and feed conditions. The inadequacy of lubrication is evident, stemming from the low MQL jet pressure and the absence of Gnps [68]. Conversely, in Figure 18b, superior surface quality is discernible, achieved through the Taguchi optimized parameters.

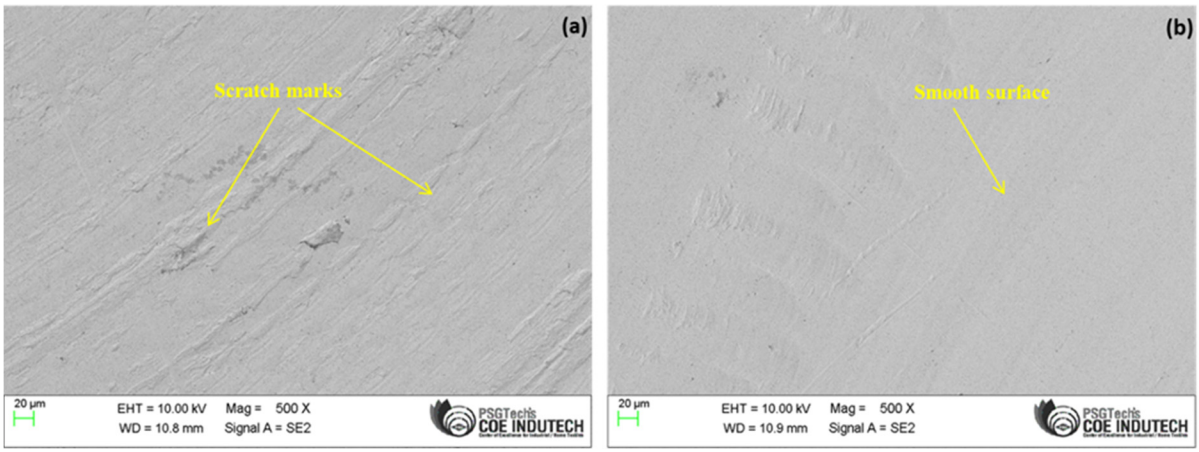

Figure 18. SEM images of machined surface. (**a**) A1-B2-C2-D1, (**b**) A2-B1-C1-D2.

The results indicated that the Taguchi optimum parameters led to a significantly improved surface quality. The percentage improvement in the performance of output variables was calculated relative to the higher values of cutting temperature and surface roughness observed in the initial cutting parameters. The results indicate a significant reduction, with a 62.5% decrease in cutting temperature and a 68.6% improvement in surface quality. This enhancement can be attributed to the GNMQL providing efficient cooling at a cutting speed of 40 m/min, feed rate of 0.01 mm/rev, and 4 bar MQL pressure condition. The positive outcome is primarily a result of the lubrication mechanism of Gnps, facilitating tribofilm formation, rolling, self-repairing, and polishing, which effectively operate under optimal cutting conditions [69]. Similarly, Mia et al. observed a reduction in surface roughness and cutting energy at Taguchi S/N ratio-based optimum cutting conditions during the end milling of AISI 4140 steel [70].

4. Conclusions

This study investigates the biodegradable sesame oil-assisted PMQL/GNMQL milling of AISI H11 steel. Based on the findings from the investigations, the following conclusions are drawn:

- Lower cutting temperatures and improved surface quality were achieved with the GNMQL cooling condition, utilizing a cutting speed of 40 m/min, a feed rate of 0.01 mm/rev, and an MQL pressure of 4 bar. In this optimized machining scenario, the GNMQL system outperformed the PMQL system due to the efficient heat dissipation facilitated by the Brownian motion and tribofilm formation of Gnps, as well as the enhanced surface quality resulting from the self-repairing and polishing actions of Gnps.
- Statistical analysis revealed that cutting speed and cooling condition had the most significant influence on milling temperature and surface smoothness, while feed rate was identified as the least influential parameter for both variables.
- The accuracy of the developed ANFIS models was 97.4% for cutting temperature and 92.6% for surface roughness.
- The optimal settings resulted in the lowest cutting temperature (51 °C) and surface roughness (0.165 μm), representing a substantial reduction of 62.5% in cutting temperature and 68.6% in surface roughness compared to the initial conditions.
- Employing Gnps with biodegradable sesame seed oil in the MQL system effectively reduced friction and lowered cutting temperatures in the cutting zone through its lubrication mechanism. Additionally, the study demonstrated that an MQL pressure of 4 bar significantly enhances efficiency in various applications.
- This study is limited in that it examines only one MQL parameter, while other factors, such as flow rate and nozzle angle, remain constant. Future research will focus on investigating the effects of varying both flow rate and nozzle angle, alongside changes in MQL jet pressure. Including these additional MQL parameters will provide a deeper insight into their effects on machining performance.
- The proposed model has the potential to deliver real-time technical support in MQL milling environments, enhancing both process efficiency and product quality by providing up-to-date insights on process parameter selection when integrated into milling operations. Future research could explore the integration of these models into the cutting process, facilitating cloud-based, real-time predictions of response parameters throughout the entire end milling operation.

Author Contributions: Formal analysis, A.B. and S.T.K.; Investigation, A.B.; Resources, S.T.K.; Data curation, S.A.; Writing—original draft, S.T.K.; Writing—review & editing, S.A.; Supervision, S.T.K. and S.A. All authors have read and agreed to the published version of the manuscript.

Funding: This research received no external funding.

Institutional Review Board Statement: We comply with ethical standards. We provide our consent to take part.

Informed Consent Statement: The authors provide consent to participate and publication.

Data Availability Statement: The authors confirm that the data supporting the findings of this study are available within the article.

Conflicts of Interest: The authors declare no conflicts of interest.

References

1. Budzynski, P.; Kara, L.; Küçükömeroglu, T.; Kaminski, M. The influence of nitrogen implantation on tribological properties of AISI H11 steel. *Vacuum* **2015**, *122*, 230–235. [CrossRef]
2. Salem, M.; Le Roux, S.; Dour, G.; Vande Put, A. Role of oxidation in thermal fatigue damage mechanisms and life of X38CrMoV5 (AISI H11) hot work tool steel. *Int. J. Fatigue* **2025**, *190*, 108584. [CrossRef]
3. Tahmasebi, E.; Albertelli, P.; Lucchini, T.; Monno, M.; Mussi, V. CFD and experimental analysis of the coolant flow in cryogenic milling. *Int. J. Mach. Tools Manuf.* **2019**, *140*, 20–33. [CrossRef]

4. Tamang, S.K.; Chandrasekaran, M.; Sahoo, A.K. Sustainable machining: An experimental investigation and optimization of machining Inconel 825 with dry and MQL approach. *J. Brazilian Soc. Mech. Sci. Eng.* **2018**, *40*, 374. [CrossRef]
5. Boswell, B.; Islam, M.N.; Davies, I.J.; Ginting, Y.R.; Ong, A.K. A review identifying the effectiveness of minimum quantity lubrication (MQL) during conventional machining. *Int. J. Adv. Manuf. Technol.* **2017**, *92*, 321–340. [CrossRef]
6. Said, Z.; Gupta, M.; Hegab, H.; Arora, N.; Khan, A.M.; Jamil, M.; Bellos, E. A comprehensive review on minimum quantity lubrication (MQL) in machining processes using nano-cutting fluids. *Int. J. Adv. Manuf. Technol.* **2019**, *105*, 2057–2086. [CrossRef]
7. Ross, N.S.; Ganesh, M.; Ananth, M.B.J.; Kumar, M.; Rai, R.; Gupta, M.K.; Korkmaz, M.E. Development and potential use of MWCNT suspended in vegetable oil as a cutting fluid in machining of Monel 400. *J. Mol. Liq.* **2023**, *382*, 121853. [CrossRef]
8. Duc, T.M.; Tuan, N.M.; Long, T.T. Optimization of Al_2O_3 nanoparticle concentration and cutting parameters in hard milling under nanofluid MQL environment. *Adv. Mech. Eng.* **2024**, *16*, 16878132241257114. [CrossRef]
9. Spandana, B.; Prasad, R.B.N.; Sarika, C.H.; Anuradha, G.; Sivaraj, N.; Sivaramakrishnan, S. Variation in seed oil content and fatty acid composition in sesame (*Sesamum indicum*). *Indian J. Agric. Sci.* **2013**, *83*, 1402–1405.
10. Uzun, B.; Arslan, C.; Karhan, M.; Toker, C. Fat and fatty acids of white lupin (*Lupinus albus* L.) in comparison to sesame (*Sesamum indicum* L.). *Food Chem.* **2007**, *102*, 45–49. [CrossRef]
11. Composition, F.A.; Arab, R.; Casal, S.; Pinho, T.; Cruz, R.; Freidja, M.L.; Lorenzo, M.; Hano, C.; Madani, K.; Boulekbache-makhlouf, L. Effects of Seed Roasting Temperature on Sesame Oil Fatty Acid Composition, Lignan, Sterol and Tocopherol Contents, Oxidative Stability and Antioxidant Potential for Food Applications. *Molecules* **2022**, *27*, 4508. [CrossRef] [PubMed]
12. Namiki, M. Nutraceutical functions of sesame: A review. *Crit. Rev. Food Sci. Nutr.* **2007**, *47*, 651–673. [CrossRef] [PubMed]
13. Padmini, R.; Vamsi Krishna, P.; Krishna Mohana Rao, G. Performance assessment of micro and nano solid lubricant suspensions in vegetable oils during machining. *Proc. Inst. Mech. Eng. Part B J. Eng. Manuf.* **2015**, *229*, 2196–2204. [CrossRef]
14. Ni, J.; Cui, Z.; Wu, C.; Sun, J.; Zhou, J. Evaluation of MQL broaching AISI 1045 steel with sesame oil containing nano-particles under best concentration. *J. Clean. Prod.* **2021**, *320*, 128888. [CrossRef]
15. Paul, G.; Hirani, H.; Kuila, T.; Murmu, N.C. Nanolubricants dispersed with graphene and its derivatives: An assessment and review of the tribological performance. *Nanoscale* **2019**, *11*, 3458–3483. [CrossRef]
16. ul Haq, M.A.; Hussain, S.; Ali, M.A.; Farooq, M.U.; Mufti, N.A.; Pruncu, C.I.; Wasim, A. Evaluating the effects of nano-fluids based MQL milling of IN718 associated to sustainable productions. *J. Clean. Prod.* **2021**, *310*, 127463. [CrossRef]
17. Gong, L.; Bertolini, R.; Ghiotti, A.; He, N.; Bruschi, S. Sustainable turning of Inconel 718 nickel alloy using MQL strategy based on graphene nanofluids. *Int. J. Adv. Manuf. Technol.* **2020**, *108*, 3159–3174. [CrossRef]
18. Bertolini, R.; Ghiotti, A.; Bruschi, S. Graphene nanoplatelets as additives to MQL for improving tool life in machining Inconel 718 alloy. *Wear* **2021**, *476*, 203656. [CrossRef]
19. Wang, H.; Bai, Q.; Chen, S.; Dou, Y.; Guo, W.; Wang, T. Performance Evaluation of Graphene Nanofluid to Mitigate the Wear of a Diamond Tool in Micro-Machining of Ti_6Al_4V Alloy. *J. Manuf. Mater. Process.* **2023**, *7*, 131. [CrossRef]
20. Marcon, A.; Melkote, S.; Kalaitzidou, K.; Debra, D. An experimental evaluation of graphite nanoplatelet based lubricant in micro-milling. *CIRP Ann. Manuf. Technol.* **2010**, *59*, 141–144. [CrossRef]
21. Baldin, V.; da Silva, L.R.R.; Houck, C.F.; Gelamo, R.V.; Machado, Á.R. Effect of graphene addition in cutting fluids applied by mql in end milling of aisi 1045 steel. *Lubricants* **2021**, *9*, 70. [CrossRef]
22. Anandan, V.; Naresh Babu, M.; Vetrivel Sezhian, M.; Yildirim, C.V.; Dinesh Babu, M. Influence of graphene nanofluid on various environmental factors during turning of M42 steel. *J. Manuf. Process.* **2021**, *68*, 90–103. [CrossRef]
23. Fisher, O.J.; Watson, N.J.; Porcu, L.; Bacon, D.; Rigley, M.; Gomes, R.L. Multiple target data-driven models to enable sustainable process manufacturing: An industrial bioprocess case study. *J. Clean. Prod.* **2021**, *296*, 126242. [CrossRef]
24. Mia, M.; Razi, M.H.; Ahmad, I.; Mostafa, R.; Rahman, S.M.S.; Ahmed, D.H.; Dey, P.R.; Dhar, N.R. Effect of time-controlled MQL pulsing on surface roughness in hard turning by statistical analysis and artificial neural network. *Int. J. Adv. Manuf. Technol.* **2017**, *91*, 3211–3223. [CrossRef]
25. Yurtkuran, H.; Korkmaz, M.E.; Gupta, M.K.; Yılmaz, H.; Günay, M.; Vashishtha, G. Prediction of power consumption and its signals in sustainable turning of PH13-8Mo steel with different machine learning models. *Int. J. Adv. Manuf. Technol.* **2024**, *133*, 2171–2188. [CrossRef]
26. Dambatta, Y.S.; Sayuti, M.; Sarhan, A.A.D.; Hamdi, M.; Manladan, S.M.; Reddy, M. Tribological performance of SiO_2-based nanofluids in minimum quantity lubrication grinding of Si_3N_4 ceramic. *J. Manuf. Process.* **2019**, *41*, 135–147. [CrossRef]
27. Gupta, M.K.; Mia, M.; Pruncu, C.I.; Khan, A.M.; Rahman, M.A.; Jamil, M.; Sharma, V.S. Modeling and performance evaluation of Al_2O_3, MoS_2 and graphite nanoparticle-assisted MQL in turning titanium alloy: An intelligent approach. *J. Brazilian Soc. Mech. Sci. Eng.* **2020**, *42*, 207. [CrossRef]
28. Saha, S.; Deb, S.; Bandyopadhyay, P.P. An analytical approach to assess the variation of lubricant supply to the cutting tool during MQL assisted high speed micromilling. *J. Mater. Process. Technol.* **2020**, *285*, 116783. [CrossRef]

29. Rohit, J.N.; Surendra Kumar, K.; Sura Reddy, N.; Kuppan, P.; Balan, A.S.S. *Computational Fluid Dynamics Analysis of MQL Spray Parameters and Its Influence on MQL Milling of SS304 [Internet]*; Lecture Notes on Multidisciplinary Industrial Engineering; Springer: Singapore, 2018; Volume Part F48, pp. 45–78. [CrossRef]
30. Peng, R.; Liu, J.; Chen, M.; Tong, J.; Zhao, L. Development of a pressurized internal cooling milling cutter and its machining performance assessment. *Precis. Eng.* **2021**, *72*, 315–329. [CrossRef]
31. Balasuadhakar, A.; Kumaran, S.T.; Uthayakumar, M. Machine learning models for enhanced cutting temperature prediction in hard milling process. *Int. J. Interact. Des. Manuf.* **2024**, *18*, 3935–3950. [CrossRef]
32. Saner, B.; Okyay, F.; Yürüm, Y. Utilization of multiple graphene layers in fuel cells. 1. An improved technique for the exfoliation of graphene-based nanosheets from graphite. *Fuel* **2010**, *89*, 1903–1910. [CrossRef]
33. Liao, Y.; Li, Z.; Fatima; Xia, W. Size-dependent structural behaviors of crumpled graphene sheets. *Carbon* **2021**, *174*, 148–157. [CrossRef]
34. Danish, M.; Gupta, M.K.; Rubaiee, S.; Ahmed, A.; Sarikaya, M. Influence of graphene reinforced sunflower oil on thermo-physical, tribological and machining characteristics of inconel 718. *J. Mater. Res. Technol.* **2021**, *15*, 135–150. [CrossRef]
35. Samy, G.S.; Thirumalai Kumaran, S.; Uthayakumar, M. An analysis of end milling performance on B4C particle reinforced aluminum composite. *J. Aust. Ceram. Soc.* **2017**, *53*, 373–383. [CrossRef]
36. Davies, M.A.; Ueda, T.; M'Saoubi, R.; Mullany, B.; Cooke, A.L. On The Measurement of Temperature in Material Removal Processes. *CIRP Ann. Manuf. Technol.* **2007**, *56*, 581–604. [CrossRef]
37. Dewes, R.C.; Ng, E.; Chua, K.S.; Newton, P.G.; Aspinwall, D.K. Temperature measurement when high speed machining hardened mould/die steel. *J. Mater. Process. Technol.* **1999**, *92–93*, 293–301. [CrossRef]
38. *ISO 21920-2:2021*; Geometrical Product Specifications (GPS)—Indication of Surface Texture in Technical Product Documentation—Part 2: Requirements for Surface Texture Symbols. International Organization for Standardization: Geneva, Switzerland, 2021.
39. Metelkova, J.; Vanmunster, L.; Haitjema, H.; Van Hooreweder, B. Texture of inclined up-facing surfaces in laser powder bed fusion of metals. *Addit. Manuf.* **2021**, *42*, 101970. [CrossRef]
40. Saklakoglu, I.E.; Kasman, S. Investigation of micro-milling process parameters for surface roughness and milling depth. *Int. J. Adv. Manuf. Technol.* **2011**, *54*, 567–578. [CrossRef]
41. Özbek, O.; Saruhan, H. The effect of vibration and cutting zone temperature on surface roughness and tool wear in eco-friendly MQL turning of AISI D2. *J. Mater. Res. Technol.* **2020**, *9*, 2762–2772. [CrossRef]
42. Hadad, M.J.; Tawakoli, T.; Sadeghi, M.H.; Sadeghi, B. Temperature and energy partition in minimum quantity lubrication-MQL grinding process. *Int. J. Mach. Tools Manuf.* **2012**, *54–55*, 10–17. [CrossRef]
43. Liu, Z.Q.; Cai, X.J.; Chen, M.; An, Q.L. Investigation of cutting force and temperature of end-milling Ti-6Al-4V with different minimum quantity lubrication (MQL) parameters. *Proc. Inst. Mech. Eng. Part B J. Eng. Manuf.* **2011**, *225*, 1273–1279. [CrossRef]
44. Sadeghi, M.H.; Haddad, M.J.; Tawakoli, T.; Emami, M. Minimal quantity lubrication-MQL in grinding of Ti-6Al-4V titanium alloy. *Int. J. Adv. Manuf. Technol.* **2009**, *44*, 487–500. [CrossRef]
45. Zaman, P.B.; Dhar, N.R. Multi-objective Optimization of Double-Jet MQL System Parameters Meant for Enhancing the Turning Performance of Ti–6Al–4V Alloy. *Arab. J. Sci. Eng.* **2020**, *45*, 9505–9526. [CrossRef]
46. Pal, A.; Chatha, S.S.; Singh, K. Performance evaluation of minimum quantity lubrication technique in grinding of AISI 202 stainless steel using nano-MoS_2 with vegetable-based cutting fluid. *Int. J. Adv. Manuf. Technol.* **2020**, *110*, 125–137. [CrossRef]
47. Gaitonde, V.N.; Karnik, S.R.; Davim, J.P. Selection of optimal MQL and cutting conditions for enhancing machinability in turning of brass. *J. Mater. Process. Technol.* **2008**, *204*, 459–464. [CrossRef]
48. Binali, R.; Demirpolat, H.; Kuntoğlu, M.; Sağlam, H. Machinability Investigations Based on Tool Wear, Surface Roughness, Cutting Temperature, Chip Morphology and Material Removal Rate during Dry and MQL-Assisted Milling of Nimax Mold Steel. *Lubricants* **2023**, *11*, 101. [CrossRef]
49. Sen, B.; Mia, M.; Krolczyk, G.M.; Mandal, U.K.; Mondal, S.P. Eco-Friendly Cutting Fluids in Minimum Quantity Lubrication Assisted Machining: A Review on the Perception of Sustainable Manufacturing. *Int. J. Precis. Eng. Manuf. Green Technol. Korean Soc. Precis. Eng.* **2021**, *8*, 249–280. [CrossRef]
50. Balasuadhakar, A.; Thirumalai Kumaran, S.; Ahmed, F. A review on the role of nanoparticles in MQL machining. *Mater. Today Proc.* **2022**, *72*, 2828–2832. [CrossRef]
51. Li, M.; Yu, T.; Zhang, R.; Yang, L.; Li, H.; Wang, W. MQL milling of TC4 alloy by dispersing graphene into vegetable oil-based cutting fluid. *Int. J. Adv. Manuf. Technol.* **2018**, *99*, 1735–1753. [CrossRef]
52. Ali, S.H.; Yao, Y.; Wu, B.; Zhao, B.; Ding, W.; Jamil, M.; Khan, A.; Baig, A.; Liu, Q.; Xu, D. Recent developments in MQL machining of aeronautical materials: A comparative review. *Chin. J. Aeronaut.* **2024**, *38*, 102918. [CrossRef]
53. Şirin, E.; Kıvak, T.; Yıldırım, Ç.V. Effects of mono/hybrid nanofluid strategies and surfactants on machining performance in the drilling of Hastelloy X. *Tribiol. Int.* **2021**, *157*, 106894. [CrossRef]
54. Cetin, M.H.; Kabave Kilincarslan, S. Effects of cutting fluids with nano-silver and borax additives on milling performance of aluminium alloys. *J. Manuf. Process.* **2020**, *50*, 170–182. [CrossRef]

55. Dhar, N.R.; Kamruzzaman, M.; Ahmed, M. Effect of minimum quantity lubrication (MQL) on tool wear and surface roughness in turning AISI-4340 steel. *J. Mater. Process. Technol.* **2006**, *172*, 299–304. [CrossRef]
56. Wang, Z.; Kovvuri, V.; Araujo, A.; Bacci, M.; Hung, W.N.P.; Bukkapatnam, S.T.S. Built-up-edge effects on surface deterioration in micromilling processes. *J. Manuf. Process.* **2016**, *24*, 321–327. [CrossRef]
57. Wojciechowski, S.; Wiackiewicz, M.; Krolczyk, G.M. Study on metrological relations between instant tool displacements and surface roughness during precise ball end milling. *Meas. J. Int. Meas. Confed.* **2018**, *129*, 686–694. [CrossRef]
58. Zhang, Y.; Li, C.; Jia, D.; Li, B.; Wang, Y.; Yang, M.; Hou, Y.; Zhang, X. Experimental study on the effect of nanoparticle concentration on the lubricating property of nanofluids for MQL grinding of Ni-based alloy. *J. Mater. Process. Technol.* **2016**, *232*, 100–115. [CrossRef]
59. Taylor, P.; Yu, W.; France, D.M.; Routbort, J.L.; Choi, S.U.S. Review and Comparison of Nanofluid Thermal Conductivity and Heat Transfer Enhancements. *Heat Transf. Eng.* **2012**, *37*, 37–41.
60. Lopes, J.C.; Garcia, M.V.; Volpato, R.S.; de Mello, H.J.; Ribeiro, F.S.F.; de Angelo Sanchez, L.E.; de Oliveira Rocha, K.; Neto, L.D.; Aguiar, P.R.; Bianchi, E.C. Application of MQL technique using TiO2 nanoparticles compared to MQL simultaneous to the grinding wheel cleaning jet. *Int. J. Adv. Manuf. Technol.* **2020**, *106*, 2205–2218. [CrossRef]
61. Sia, S.Y.; Sarhan, A.A.D. Morphology investigation of worn bearing surfaces using SiO_2 nanolubrication system. *Int. J. Adv. Manuf. Technol.* **2014**, *70*, 1063–1071. [CrossRef]
62. Wang, X.; Li, C.; Zhang, Y.; Ding, W.; Yang, M.; Gao, T.; Cao, H.; Xu, X.; Wang, D.; Said, Z.; et al. Vegetable oil-based nanofluid minimum quantity lubrication turning: Academic review and perspectives. *J. Manuf. Process.* **2020**, *59*, 76–97. [CrossRef]
63. Gürbüz, H.; Emre Gönülaçar, Y. Optimization and evaluation of dry and minimum quantity lubricating methods on machinability of AISI 4140 using Taguchi design and ANOVA. *Proc. Inst. Mech. Eng. Part C J. Mech. Eng. Sci.* **2021**, *235*, 1211–1227. [CrossRef]
64. Karaboga, D.; Kaya, E. Adaptive network based fuzzy inference system (ANFIS) training approaches: A comprehensive survey. *Artif. Intell. Rev.* **2019**, *52*, 2263–2293. [CrossRef]
65. Al-Mahasneh, M.; Aljarrah, M.; Rababah, T.; Alu'datt, M. Application of Hybrid Neural Fuzzy System (ANFIS) in Food Processing and Technology. *Food Eng. Rev.* **2016**, *8*, 351–366. [CrossRef]
66. Hájek, P.; Olej, V. Adaptive Intuitionistic Fuzzy Inference Systems of Takagi-Sugeno Type for Regression Problems. In Proceedings of the Artificial Intelligence Applications and Innovations: 8th IFIP WG 12.5 International Conference, AIAI 2012, Halkidiki, Greece, 27–30 September 2012; pp. 206–216.
67. Yeom, C.U.; Kwak, K.C. Performance comparison of ANFIS models by input space partitioning methods. *Symmetry* **2018**, *10*, 700. [CrossRef]
68. Masoudi, S.; Esfahani, M.J.; Jafarian, F.; Mirsoleimani, S.A. Comparison the Effect of MQL, Wet and Dry Turning on Surface Topography, Cylindricity Tolerance and Sustainability. *Int. J. Precis. Eng. Manuf. Green Technol.* **2023**, *10*, 9–21. [CrossRef]
69. Niknam, S.A.; Jalali, A. Effects of lubricants and flow rates on the surface roughness and chip thickness when MQL turning of aero-engine aluminum alloys 6061-T6 and 7076-T6. *Int. J. Adv. Manuf. Technol.* **2020**, *110*, 2015–2022. [CrossRef]
70. Mia, M. Mathematical modeling and optimization of MQL assisted end milling characteristics based on RSM and Taguchi method. *Meas. J. Int. Meas. Confed.* **2018**, *121*, 249–260. [CrossRef]

Disclaimer/Publisher's Note: The statements, opinions and data contained in all publications are solely those of the individual author(s) and contributor(s) and not of MDPI and/or the editor(s). MDPI and/or the editor(s) disclaim responsibility for any injury to people or property resulting from any ideas, methods, instructions or products referred to in the content.